

Received November 18, 2017, accepted December 17, 2017, date of publication December 27, 2017, date of current version February 28, 2018.

Digital Object Identifier 10.1109/ACCESS.2017.2787724

# Origami Segmented Helical Antenna With Switchable Sense of Polarization

SHUN YAO, (Student Member, IEEE),  
AND STAVROS V. GEORGAKOPOULOS<sup>1</sup>, (Senior Member, IEEE)

Department of Electrical and Computer Engineering, Florida International University, Miami, FL 33174, USA

Corresponding author: Stavros V. Georgakopoulos (georgako@fiu.edu)

This work was supported by the National Science Foundation under Grant EFRI 1332348.

**ABSTRACT** A new design of a segmented helical antenna (SHA), which can switch its sense of polarization by rotating around its center axis is presented. Two implementation methods, one based on origami folding and the other one based on skeleton scaffolding are developed. Example bifilar SHA designs are presented for the UHF frequency band. The performance of the antennas is studied and validated through simulations and measurements. Specifically, the reflection coefficient, axial ratio, realized gain, and radiation pattern beamwidth of the proposed SHAs are investigated and compared with the ones of a conventional bifilar helical antenna. The proposed SHA has two stable states of operation, one with right-hand circular polarization and the other one with left-hand circular polarization. The sense of the polarization of this antenna can be controlled and switched using mechanical rotation. Therefore, this antenna exhibits reconfigurable polarization performance.

**INDEX TERMS** Helical antenna (HA), segmented helical antenna (SHA), reconfigurable antenna, origami antenna, origami, bifilar, RHCP, LHCP.

## I. INTRODUCTION

Axial mode conventional helical antennas (HAs) have been widely used in satellite communications and global positioning systems due to their high gain and circular polarization. The properties of conventional helical antennas have been extensively studied. Segmented helical antennas (SHAs), such as square cross section helical antennas, have been investigated in [1]–[3]. SHAs can provide approximately equivalent performance compared to the conventional helical antenna. The linear segments, which make up a SHA can be easily supported on a dielectric structure. This kind of structure can be designed and manufactured at a very low cost.

The physical size of helical antennas becomes considerably large at lower frequencies and requires a strong mechanical support. Several methods to reduce the total antenna volume have been developed and studied. A dielectric rod inside the helix was introduced in [4] and [5]. The volume of such antenna is tremendously decreased by 95%, but the gain is also decreased (below 4 dBi). Placing radial stubs along the circumference of the helix without affecting the radiation characteristics of the antenna was studied in [6] and [7]. The stubs increase the electrical length of antennas, and

40%–70% antenna volume reduction is achieved. However, the stubs change the input impedance of the antenna and a matching network is necessary in such designs. Meandering radiating elements of the helical antenna were used in [8]–[11]. The volume of these antennas was approximately 50% smaller compared to traditional helical antennas, but the axial ratio and the beamwidth of these antennas were compromised.

Deployable helical antennas for CubeSats have been investigated recently [12]–[14]. Bifilar and quadrifilar HAs, which have better gain and lower beamwidth than a monofilar HA, are used in these designs. These antennas are composed of conductors that are supported by novel structures. This allows efficient folding, packaging, and deployment in space. In [12], a UHF quadrifilar helical antenna, supported by helical arms of S2 glass fiber reinforced epoxy, was designed. The structure has the potential to deploy itself by releasing its stored strain energy. Origami based helical antennas have been developed in [13] and [14]. The origami helical antennas have comparable performance to conventional helical antennas. Also, origami helical antennas can operate at different frequency bands by adjusting the height of the origami cylinders that support them.

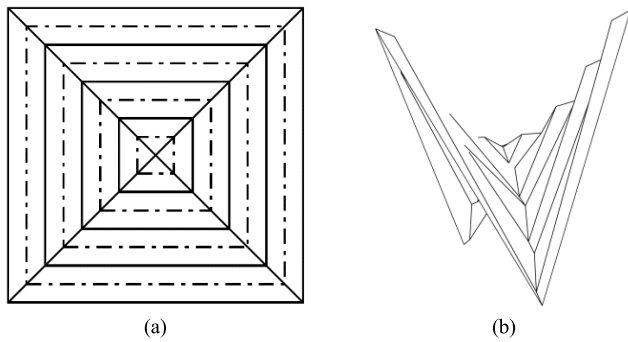


**FIGURE 1.** (a) Creased square pattern for hyperbolic paraboloid origami. (b) Hyperbolic paraboloid origami.

Most circular polarized (CP) helical antennas only have one sense of polarization: right-hand circular polarization (RHCP) or left-hand polarization (LHCP). The sense of CP field of the helical antenna is determined by the direction of twist of the helix arms. In some applications, dual-band reception of both RHCP and LHCP signals are required. Dual sense CP antennas have been investigated, such as cross dipole antennas [15] and slot antennas [16]. In such antennas, the directions of the peak gain at the two states are opposite, and the gain is low (below 4 dBi). CP sense switchable antennas have also been developed in [17] and [18]. These antennas need extra switching circuits and power supplies.

In this paper, a new SHA design with switchable sense of polarization is presented. In Section II, the hyperbolic paraboloid origami structure, which is used for this SHA design, is presented and analyzed. In Section III, an origami SHA with switchable polarization is developed, and its performance is compared with the performance of conventional HAs. In Section IV, an SHA based on a skeleton scaffolding and with switchable polarization is described, this design is inspired by the origami SHA. In Section V, prototypes of the skeleton SHA are manufactured, and their performance is validated through simulations and measurements.

## II. THE HYPERBOLIC PARABOLOID ORIGAMI UNIT FOR ORIGAMI SHA

The hyperbolic paraboloid origami structure, as shown in Fig. 1, was originally developed in 1928 at Bauhaus [19]. This hyperbolic paraboloid can be created by taking a square piece of paper and folding the diagonals and concentric squares in alternating direction, i.e., a square of mountain folds depicted in Fig. 1(a) by the solid lines, followed by a square of valley folds depicted by the dash lines in Fig. 1(a), and so on. After following this process, the paper pops automatically into a saddle curve [20]. Non-squares hyperbolic paraboloid origami structures have also been developed by Demaine *et al.* [20].

A new 3D structure can be developed by connecting several rectangle hyperbolic paraboloid origami structures in series, as shown in Fig. 2(a). This structure can be used as a base for a

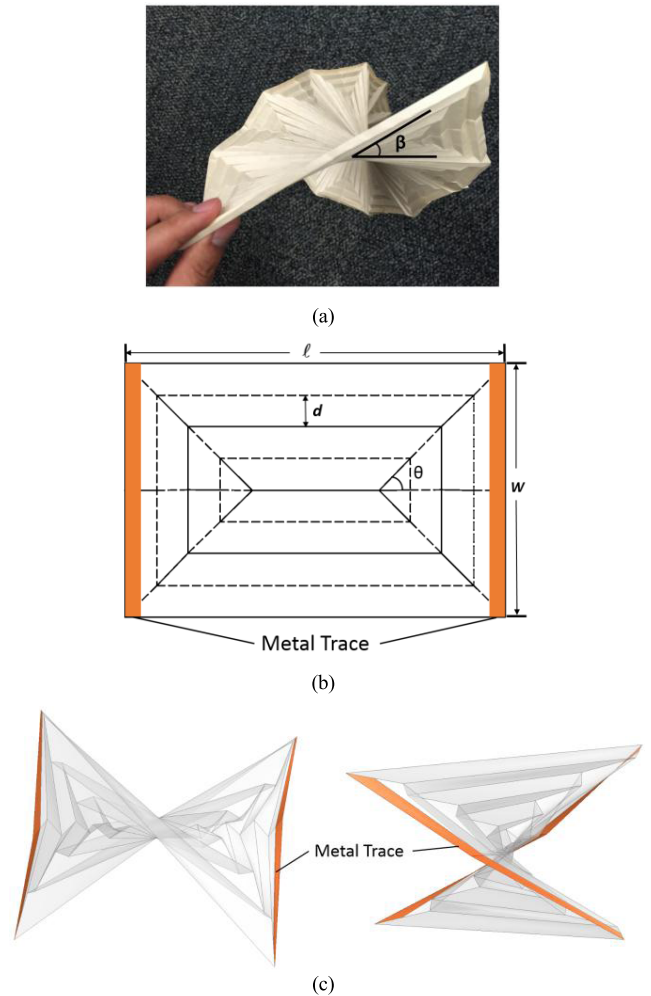


**FIGURE 2.** (a) Origami paper base that can rotate around its center axis with multiple hyperbolic paraboloid units. (b) The origami rectangle unit pattern for the hyperbolic paraboloid with the antenna traces. (c) Top view and side view of a rectangle hyperbolic paraboloid origami unit with the antenna traces.

new origami segmented helical antenna with switchable sense of polarization [21]. This new antenna consists of a series of identical rectangle hyperbolic paraboloid origami units where the two side edges of each unit have the segmented antenna trace, as shown in Figs. 2(b) and 2(c). This new antenna has two stable states (bi-stable design): a left-handed and a right-handed state. By fixing the bottom edge of each unit and rotating its top edge, each origami unit can pop from one state to the other.

Fig. 2(b) shows the rectangle origami unit. The solid lines are mountain-folds, and the dash lines are valley-folds. The lines of each rectangle alternate from solid to dashed. The length of each origami unit is  $\ell$ , and the width of each origami unit is  $w$ . The number of rectangles in each unit is  $m$ , in Fig. 2(b),  $m = 4$ . The distance  $d$  between the adjacent rectangles should be identical. The rotation angle  $\beta$  of each unit, which is shown in Fig. 2(a), is determined by the ratio  $\ell/w$  and the number  $m$ . The larger the ratio  $\ell/w$  is,

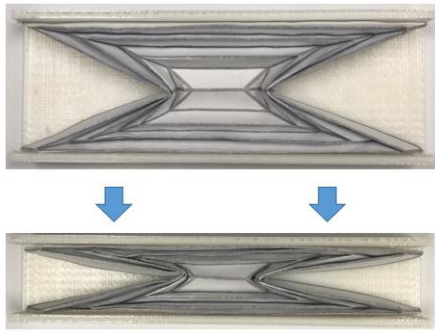


**FIGURE 3.** Rectangle hyperbolic paraboloid origami unit at the compact intermediate state for stowing.

the smaller  $\beta$  will be. Also, the fewer rectangles in each unit, the smaller  $\beta$  will be.

When the angle  $\theta$ , shown in Fig. 2(b), equals  $45^\circ$ , the rectangle hyperbolic paraboloid origami unit can collapse its height. In this case, the origami unit can be compressed as a collapsible spring, as shown in Fig. 3. This collapsible state of the paraboloid is not stable, but it can be used to stow the origami structure compactly and therefore it can be an intermediate non-operational state.

For our example origami SHA design in this paper, which will be presented in next section, the length,  $\ell$ , of the origami unit equals 100 mm. Each unit has 7 rectangles and a width,  $w$ , of 84 mm. The distance,  $d$ , is 6 mm, and the height of each folded unit is approximately 20 mm. The metal trace is attached along the two short sides of each rectangle origami unit. If the paper base has  $n$  rectangle origami units, then the total length of metal trace will be  $nw$ , and the number of turns,  $N$ , of the SHA will be

$$N = n\beta/2\pi \tag{1}$$

Materials with different thicknesses were tested for this origami unit. The origami base must be thick enough to mechanically support the hyperbolic paraboloid structure, but if it becomes too thick it will not be foldable. Fig. 4 shows the rectangle hyperbolic paraboloid origami unit for the left-handed and right-handed states for different materials (paper and Kapton<sup>®</sup>) and different thicknesses. The thickness of the material has a small effect on the rotation angle  $\beta$ . The thicker the material is, the smaller  $\beta$  will be. From our experiment results, the applicable thickness range for the commercially available paper without any coating is from  $100 \mu\text{m}$  to  $400 \mu\text{m}$ . For our example design in this paper,  $100 \mu\text{m}$ -thick paper is used as the origami base. The rotation angle,  $\beta$ , of the  $100 \mu\text{m}$ -thick paper origami unit is approximately  $90^\circ$ . The origami units that were built with Kapton<sup>®</sup> FPC film exhibit similar properties compared to the paper base. The applicable thickness range for the Kapton films is from  $50 \mu\text{m}$  to  $150 \mu\text{m}$ . The 2 mil-thick Kapton unit, shown in Figs. 4(c) and 4(d), has the biggest rotation angle  $\beta$ . The 5 mil-thick Kapton unit, shown in Figs. 4(g) and 4(h), has the most stable structure.

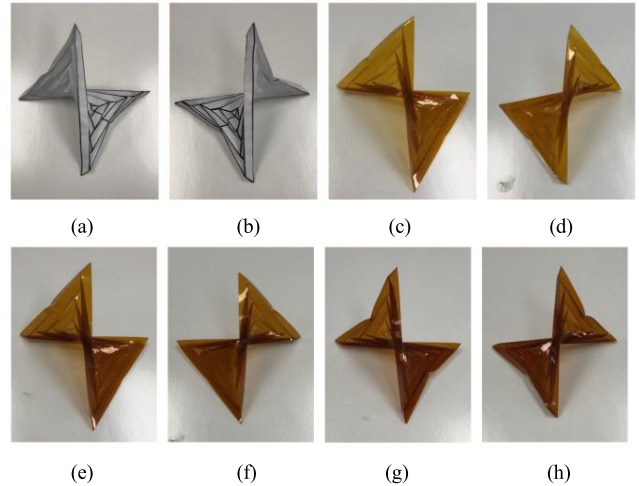


**FIGURE 4.** The hyperbolic paraboloid origami unit for (a)  $150 \mu\text{m}$ -thick paper at left-hand state, (b)  $150 \mu\text{m}$ -thick paper at right-hand state, (c)  $50 \mu\text{m}$ -thick (2-mil) Kapton film at left-hand state, (d)  $50 \mu\text{m}$ -thick (2-mil) Kapton film at right-hand state, (e)  $76 \mu\text{m}$ -thick (3-mil) Kapton film at left-hand state, (f)  $76 \mu\text{m}$ -thick (3-mil) Kapton film at right-hand state, (g)  $127 \mu\text{m}$ -thick (5-mil) Kapton film at left-hand state, and (h)  $127 \mu\text{m}$ -thick (5-mil) Kapton film at right-hand state.

### III. ORIGAMI SEGMENTED HELICAL ANTENNA

An origami Segmented Helical Antenna (SHA) is developed using multiple connected in series rectangle hyperbolic paraboloid origami units, which were discussed in the previous section. This origami geometry will allow a right-handed SHA to be switched to a left-handed SHA by rotating all its origami units clockwise and the left-handed SHA to be switched back to the right-handed SHA by rotating all its origami units counterclockwise. Therefore, this origami SHA can provide a switchable sense of polarization.

In this section and as an example, the performance of an origami bifilar SHA is investigated using simulations and measurements. The equivalent conventional bifilar helical antenna, which has the same diameter and height as the ones of the origami SHA, is analyzed and used as a reference.

Fig. 5 shows the side and top views of the simulation models of the origami SHA and the conventional HA that will be examined. The origami paper base is not shown in Fig. 5 in order to clearly show the antenna trace. The blue and red strips in Figs. 5(a) and 5(c) are the two metal traces of the SHA. Each metal trace is connected to a 50 ohm excitation. The two excitation ports have  $180^\circ$  phase difference. A  $150 \text{ mm}$  by  $150 \text{ mm}$  ground plane is used. This origami SHA is composed by 8 origami rectangle units ( $n = 8$ ). The rotation angle,  $\beta$ , of each origami unit is  $90^\circ$ . The number of turns,  $N$ , of this SHA can be calculated from equation (1), which is two. The total height of the origami antenna is  $160 \text{ mm}$ , and the length of each metal strip is  $672 \text{ mm}$ . Fig. 5(c) shows that the cross section of this SHA is a symmetrical polygon with 8 edges. The length of each edge is  $42 \text{ mm}$ , which is half of the width of the origami unit. The pitch angle,  $\alpha$ , of the origami SHA can be calculated

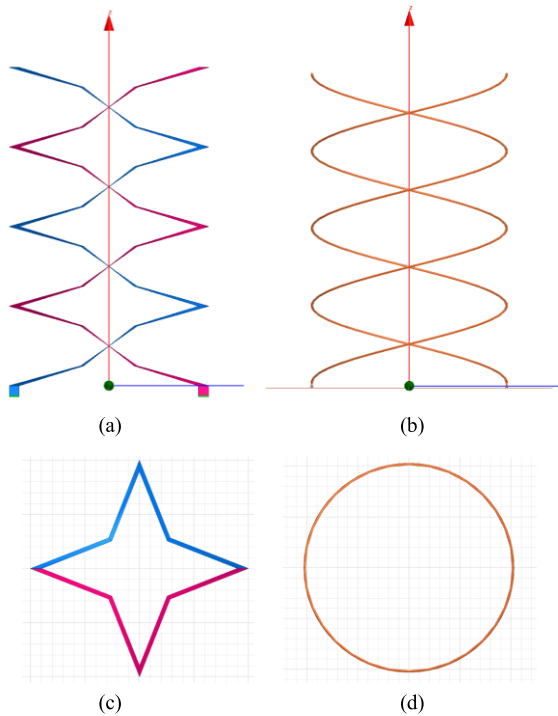


**FIGURE 5.** The side view of (a) the origami SHA, and (b) the conventional HA. The top view of (c) the origami SHA, and (d) the conventional HA.

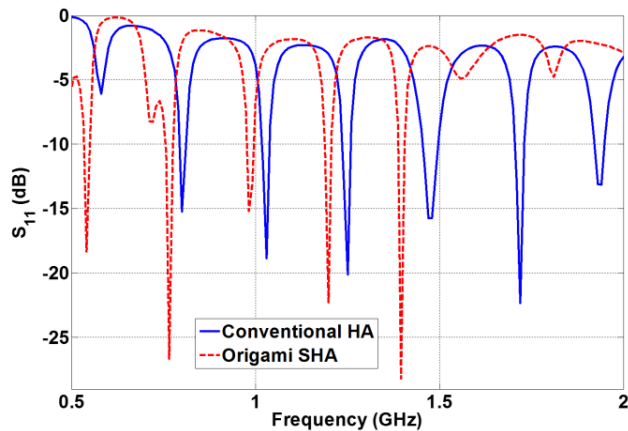


**FIGURE 6.** Simulated  $S_{11}$  of the conventional HA and origami SHA.

by:

$$\alpha = \tan^{-1} \left( \frac{\text{Antenna Height}}{n \times w} \right) \quad (2)$$

which is  $13.4^\circ$ . The conventional HA, shown in Figs. 5(b) and 5(d), also has two turns. The circumference of the conventional HA is  $\pi \ell$ . The spacing,  $S$ , between each turn is 80 mm. Therefore, the pitch angle  $\alpha$  for the conventional HA is calculated as  $14.2^\circ$ .

Fig. 6 shows the simulated reflection coefficient of the conventional HA and the origami SHA. It can be observed that the two curves are similar, and both antennas have several resonant frequencies.

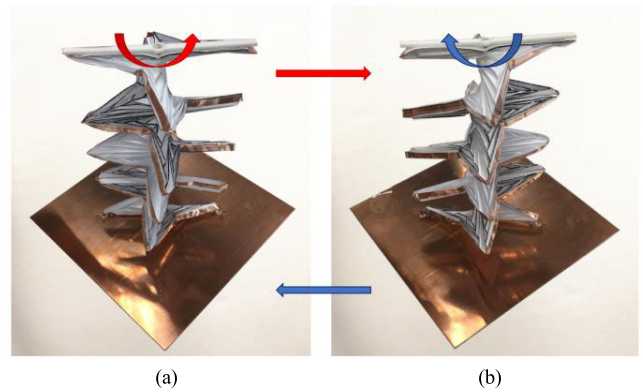


**FIGURE 7.** The manufactured prototype of origami SHA at (a) left-handed state and (b) right-handed state.

Fig. 7 shows the manufactured prototype at the left-handed state and the right-handed state. The prototype is constructed using  $50 \mu\text{m}$ -thick copper tape on  $100 \mu\text{m}$ -thick sketching-paper substrate without any coating. The copper tape is glued on the paper and creased with the paper, so that it will stay attached to the paper substrate when the antenna is rotating. The width of the copper trace is 3 mm. The two copper traces are fed using SMA connectors. The feeding network adopted for the prototypes used a broadband  $180^\circ$  hybrid coupler. A central support post is placed in the center axis of the origami structure, which goes through the center of each origami paper unit. An arm made of polylactic acid (PLA) is fixed on the top of this post, and glued at the top edge of the origami paper base, as shown in Figs. 7 and 8. The entire origami base can be rotated around its central axis by rotating the PLA arm. When the PLA arm rotates by  $2N\pi$ , which is  $720^\circ$  in this example design, the antenna switches from its right-handed state to its left-handed state.

A telescoping metal post is used as a central support post of the origami SHA, as shown in Fig. 8. From our simulation results, the metal post has negligible effects on the radiation properties of the origami SHA. The height of the antenna can be changed from 70 mm to 160 mm. The origami SHA can be tightly folded into a  $100 \text{ mm} \times 70 \text{ mm} \times 5 \text{ mm}$  volume, as shown in Fig. 8(c). Therefore, when telescopic post collapses, the volume of the origami SHA is decreased by 96% compared to the cylindrical volume of the conventional helical antenna.

The measured reflection coefficients and the simulation results for both the left-handed state and right-handed state of the origami SHA are shown in Fig. 9. It can be seen that the two states have almost identical measured  $S_{11}$ -parameters and the origami SHA has four resonant frequencies from 0.7 GHz to 1.4 GHz. The origami SHA has a narrow operating frequency band. The simulated reflection coefficients at the four operating frequencies are less than  $-15 \text{ dB}$ . The measured  $S_{11}$  is less than  $-10 \text{ dB}$  at the first three operating frequencies. The slight disagreement between the measured and simulated reflection coefficient is due to the fact that the simulated

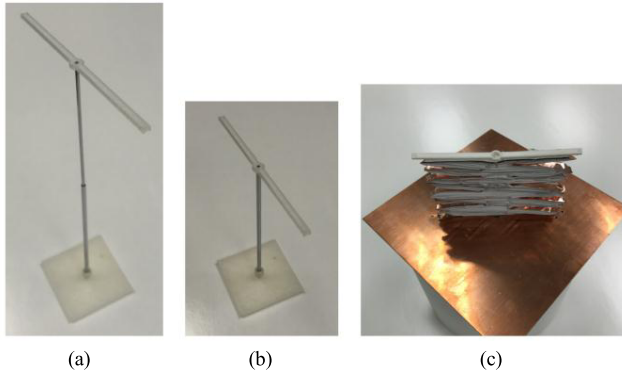


FIGURE 8. (a) Expanded telescoping central axis, (b) Collapsed telescoping central axis, (c) Tightly folded origami SHA.

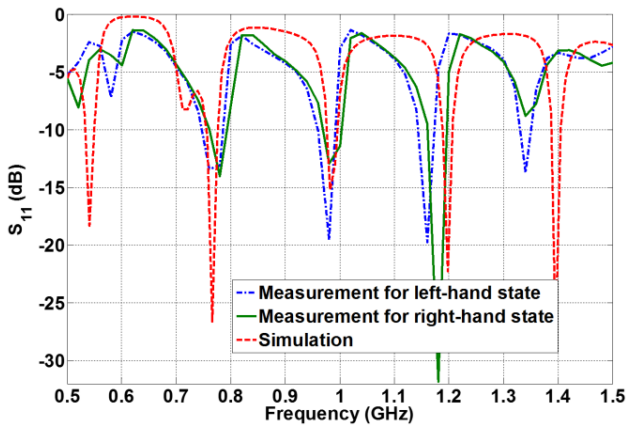


FIGURE 9. Measured  $S_{11}$  of the origami based SHA at both left-hand state and right-hand state.

origami antenna is based on an ideal centrosymmetric model, which cannot be exactly realized by the prototype, since it was built manually. Also, the slight differences between the measured  $S_{11}$ -parameters for the two states can be attributed to the fact that the origami paper base is constructed manually and, therefore, the geometries of the two states are not identical.

This SHA exhibits directional gain performance at these frequencies as shown in Fig. 10. Table 1 shows the measured far-field performance metrics of the prototyped origami SHA at the four frequencies. The far-field measurements were performed using a StarLab anechoic chamber. The results illustrate that the origami SHA has the best axial ratio (0.94 dB) and highest co-polarization realized gain (6.82 dBi) at 0.98 GHz. The comparison of the far-field characteristics between the origami SHA and the conventional HA will be discussed in Section V.

Fig. 10 shows the measured RHCP and LHCP elevation pattern of the origami SHA for  $\varphi = 0^\circ$  and  $\varphi = 90^\circ$  for both the left-handed and the right-handed states at 0.98 GHz. Fig. 10 illustrates that the origami SHA works in the axial mode, and the maximum gain is along its central axis. The level of cross-polarization gain is approximately 16 dB lower

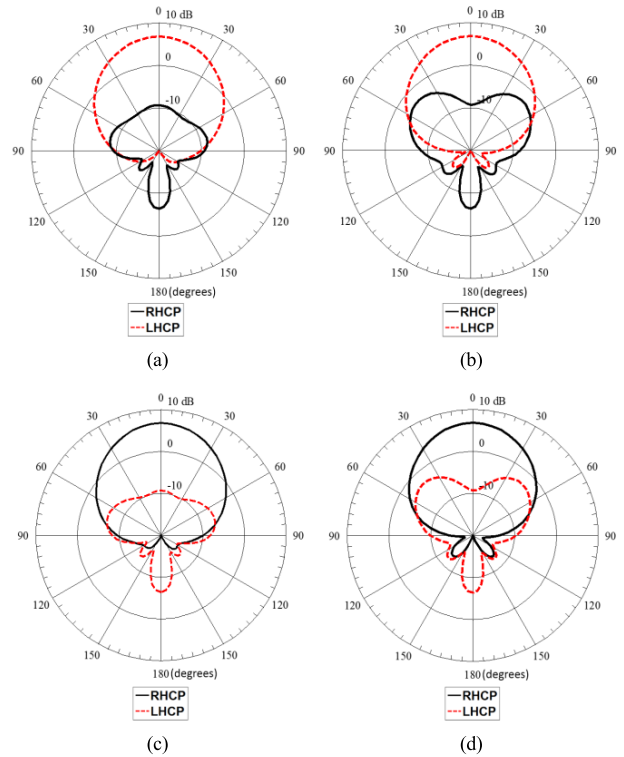


FIGURE 10. Measured elevation patterns of the origami SHA for the RHCP and LHCP components of the electric field at 0.98 GHz: (a)  $\varphi = 0^\circ$  at the left-hand state, (b)  $\varphi = 90^\circ$  at the left-hand state, (c)  $\varphi = 0^\circ$  at the right-hand state, and (d)  $\varphi = 90^\circ$  at the right-hand state.

TABLE 1. Measured far-field characteristics of origami SHA.

Far-field Characteristics	0.77 GHz	0.98 GHz	1.2 GHz	1.34 GHz
Axial Ratio	14.3 dB	0.94 dB	2.75 dB	4.46 dB
Co-polarization Realized Gain	2.68 dBi	6.82 dBi	5.35 dBi	5.77 dBi
Cross-polarization Realized Gain	-0.72 dBi	-9.28 dBi	-23.29 dBi	-6.22 dBi
E-plane HPBW	63°	62°	95°	79°
H-plane HPBW	82°	69°	91°	84°

than the co-polarization gain over the main beam direction. The shape of the radiation patterns at the two states are almost identical. The sense of polarization of this origami SHA can be switched from RHCP and LHCP by rotating the antenna around its axis to change the right-handed helix to a left-handed helix thereby providing a reconfigurable polarization.

As previously mentioned in Section II, when the crease pattern is created and folded on the paper base, each origami paper unit will have a steady state. It could pop from left-handed state to the right-handed state with identical unit height and the rotation angle  $\beta$ , which ensures the stability of the geometry of the origami SHA. However, after the paper base is compressed and deployed as shown in Fig. 8, we found that it is difficult for each origami unit to maintain the unified height. This is due to the nature of the paper material. To solve

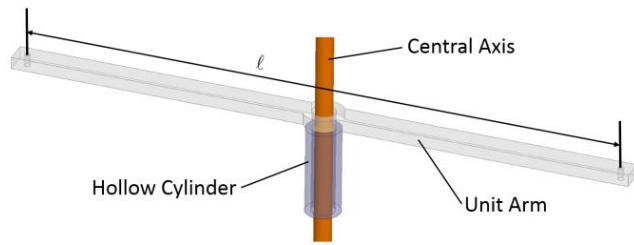


FIGURE 11. Unit of the supporting skeleton of the SHA.

this problem, the skeleton scaffolding based SHA is presented in the next section. Also, other flexible materials will be studied by our future research.

#### IV. SHA ON ORIGAMI-INSPIRED SKELETON SCAFFOLDING

Inspired by the origami SHA, which was presented in the previous section, a new SHA is developed based on a rotatable skeleton scaffolding. Fig. 11 shows the unit of the skeleton scaffolding of this SHA. A cylindrical axis goes through the central hole of the arm, and the arm can rotate around this axis [22]. There are circular holes at two ends of the arm. Copper wire feeds through these holes to construct the segmented helix. A hollow cylinder, which controls the unit height, is placed around the central axis between two adjacent arms. The arm and the hollow cylinder are shown in Fig. 11, and they both can slide up and down along the central axis. The distance between the two holes of the arm is denoted as  $\ell$ , which is geometrically equivalent to the length of the origami unit presented in Section II. It also equals the length of the diagonal line of the segmented helix's cross section. The height of each unit is denoted as  $h$ . The thickness of the arm is denoted as  $t_1$ , which determines the minimum volume of this antenna when it is collapsed (the collapsible skeleton SHA is presented in next section). The range of the rotation angle  $\beta$  between adjacent arms is between  $0^\circ$  to  $180^\circ$ .

As examples, two skeleton SHAs are designed here: a hexagon skeleton SHA and a square skeleton SHA. Both SHAs have the same geometrical size as the origami SHA presented in the previous section. The length,  $\ell$ , of the arm is 100 mm, and the total height of the antenna is 160 mm. Their simulation 3-D models are shown in Fig. 12 for both the right-handed and left-handed states. Both SHAs have a total of 2 turns.

The thickness of each arm is 2mm. Copper wire with 0.4 mm diameter feeds through a hole at one end of one arm and through the hole at the end of the next arm. The symmetrical bifilar segmented helix structure is built with the skeleton arms. Each copper wire is connected at the base of the antenna to a 50 ohm excitation, and the other end of each copper wire is fixed on the top arm. The two excitation ports have  $180^\circ$  phase difference. A 150 mm by 150 mm square copper sheet is used as the ground plane. The skeleton SHA has two states: right-handed state and left-handed state.

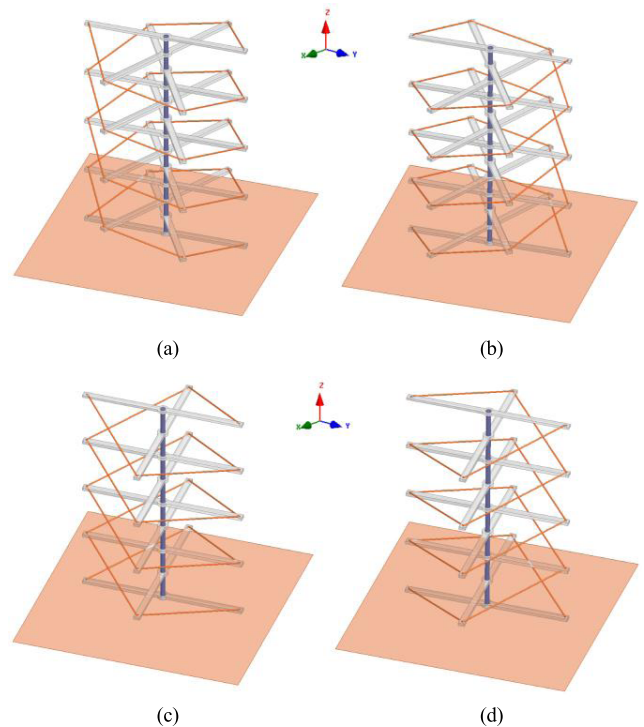


FIGURE 12. The simulation model of (a) the hexagon SHA at left-hand state, (b) the hexagon SHA at right-hand state, (c) the square SHA at left-hand state and (d) the square SHA at right-hand state.

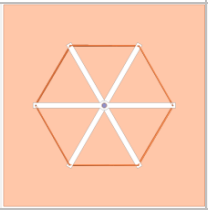
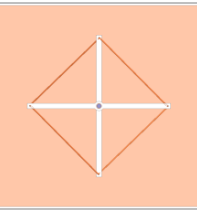
One of the advantages of this symmetrical skeleton structure is that the whole skeleton can be rotated around the central axis by only rotating the top arm, while all the rest arms are pulled by the copper wire to rotate. A right-handed skeleton SHA can be switched to a left-handed skeleton SHA by rotating the top arm  $720^\circ$  (two turns). Also, when the distances between adjacent arms are identical, the angles between adjacent arms will be identical. When the top arm is fixed on the central axis, a simple motor system can achieve the rotation operation. A video showing the skeleton SHA prototype rotating is attached as a supplement to our paper.

Table 2 shows the geometric parameters of the hexagon and square skeleton SHAs that are shown in Fig. 12. The square skeleton SHA has fewer arms, larger unit height and shorter copper wire length compared to the hexagon skeleton SHA. The pitch angle,  $\alpha$ , of these two skeleton SHAs can be calculated by equation (2). The performance of the two antennas is examined in the next section.

#### V. SKELETON SHA PERFORMANCE

In this section, prototypes of the two skeleton SHAs with the geometric parameters of Table 2 are built. Fig. 13 shows the prototypes of the skeleton SHAs and the conventional HA. In order to make the conventional HA have the standard geometry, a 3 mm thick hollow cylinder base with helical groove lines is used as support. The central axis, hollow cylinder, and arms of the skeleton scaffolding were printed with PLA filament using a 3D printer. The dielectric constant

**TABLE 2.** Geometry parameters of the segmented helical antennas.

Geometric Parameters	Hexagon Segmented Helical Antenna	Square Segmented Helical Antenna
Top View		
Number of Turns, $N$	2	2
Antenna Height	160 mm	160 mm
Number of Units, $n$	12	8
Angle Between the Adjacent Arms	60°	90°
Unit Height, $h$	13.3 mm	20 mm
Segment Length	51.75 mm	73.5 mm
Total Length of Each Copper Wire	621 mm	588 mm

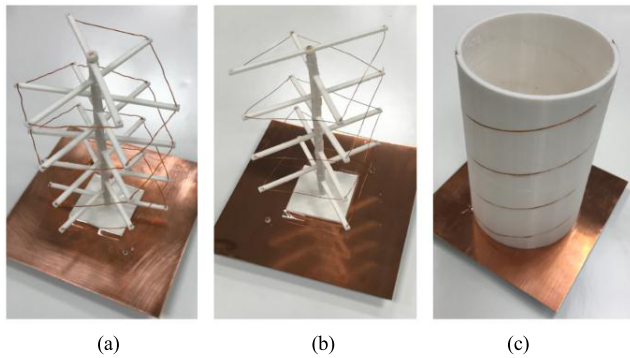


**FIGURE 13.** Manufactured prototype of the (a) hexagon skeleton SHA, (b) square skeleton SHA, and (c) conventional HA.

of the PLA is 2.5. The copper 26-gauge wire (0.409 mm diameter) used in the prototype is magnet wire with polyester coating. The thickness of the insulation layer is 0.023 mm. It should be pointed out that our simulation results show that the PLA cylinder base has negligible impact of the gain and polarization performance of the conventional HA, but it does shift its operating frequency approximately 8 MHz compared to the case with no base. The two segmented helical elements of each SHA antenna are fed using SMA connectors and with 180° phase difference between them. When the top arm rotates 720°, the entire segmented helical structure will rotate from its right-handed state to left-handed state.

The measured performance characteristics of the proposed skeleton SHAs are compared with the ones of the origami SHA and the equivalent conventional bifilar HA in Table 3. All the antennas have the same diameter, height, and number of turns. The operating frequency of each antenna is picked so that it operates in axial mode and with the best axial ratio. From the results in Table 3, it can be concluded

**TABLE 3.** Comparison between the SHAs and the conventional HA.

Antenna Characteristics	Skeleton Hexagon SHA	Skeleton Square SHA	Origami SHA	Conventional HA
Pitch Angle	14.4°	15.2°	13.4°	14.2°
Operating Frequency	1.08 GHz	1.16 GHz	0.98 GHz	1.03 GHz
Reflection Coefficient	-18 dB	-17 dB	-13 dB	-18 dB
Axial Ratio	0.74 dB	1.12 dB	0.94 dB	0.72 dB
Co-polarization Realized Gain	8.1 dBi	7.73 dBi	6.82 dBi	8.22 dBi
Cross-polarization Realized Gain	-11.32 dBi	-13.96 dBi	-9.28 dBi	-9.76 dBi
E-plane HPBW	55°	58°	62°	57°
H-plane HPBW	56°	57°	69°	56°

that all the SHAs have CP performance with small axial ratio (below 1.2 dB). The origami SHA has 1.4 dB lower gain, larger axial ratio and wider beamwidth than the corresponding ones of the conventional HA. The half-power beamwidths (HPBWs) of the radiation pattern of the two skeleton SHAs are approximately the same to the ones of the conventional HA. The two skeleton SHAs have slightly lower realized gain and slightly larger axial ratio compared to the ones of the conventional HA. Also, since the circumference of the hexagon skeleton SHA has more sides than that of the square skeleton SHA, the hexagon skeleton SHA is geometrically more similar to the conventional HA and therefore, it is expected that the axial ratio and gain performances of the hexagon skeleton SHA will be more similar to the ones of the conventional SHA. The operating frequency of the origami SHA is approximately the same to the operating frequency of the conventional HA. Whereas, the operating frequencies of the skeleton SHAs are slightly higher than the operating frequency of the conventional HA. This happens because the circumference of the skeleton SHAs are smaller than the circumference of the conventional HA. The operating frequencies of the skeleton SHAs can be decreased by increasing the length of their arms.

Fig. 14 compares the measured RHCP and LHCP elevation pattern for  $\varphi = 0^\circ$  and  $\varphi = 90^\circ$  for the skeleton SHAs at both the right-handed state and the left-handed state. The prototypes were measured in a StarLab anechoic chamber at the operating frequencies of the SHAs (i.e., the hexagon SHA was measured at 1.08 GHz, and the square SHA was measured at 1.16 GHz). It is evident that both antennas work in the axial mode, and the maximum gain is along their central axis. The level of cross-polarization gain is approximate 20 dB lower than the co-polarization gain over the main beam direction. The RHCP and LHCP gain can be switched when the skeleton SHAs are rotated from their right-handed state to their left-handed state. The slight difference between the pattern shapes at the two states can be attributed to the fact that the physical structure of the copper wire is not exactly the same at the two states.

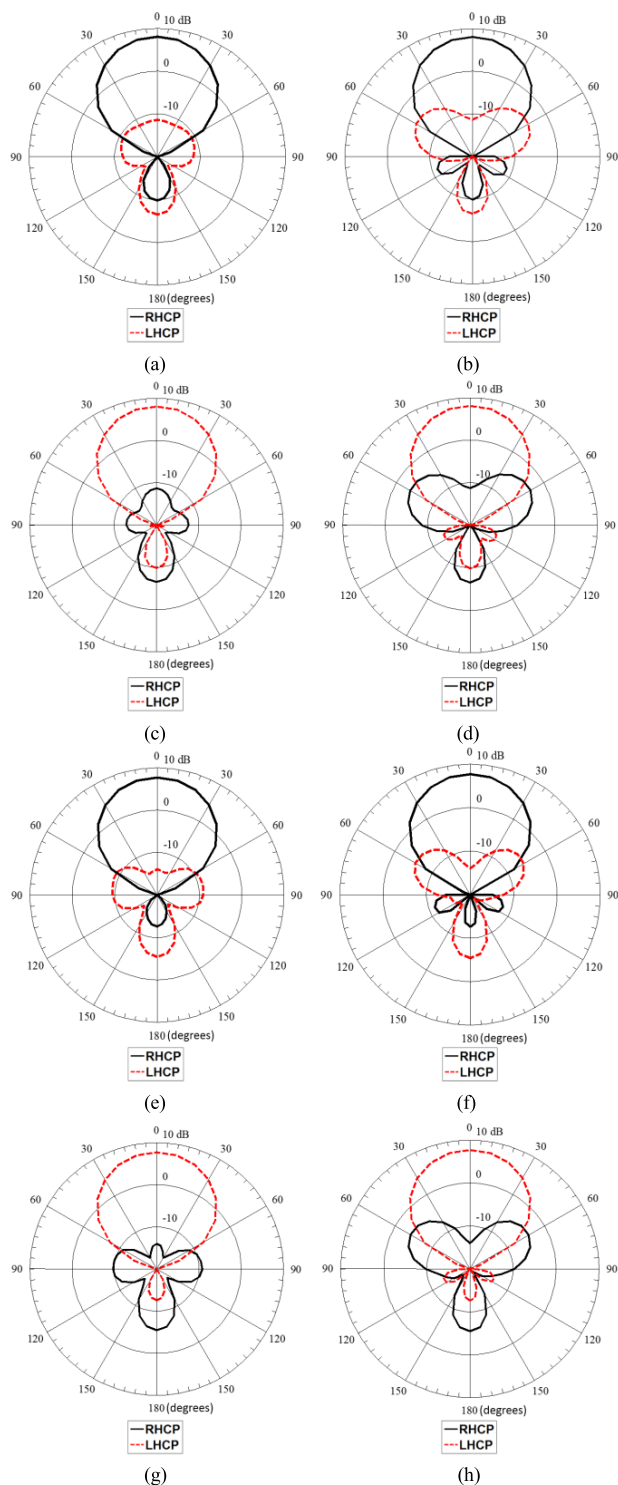


**FIGURE 14.** Measured elevation patterns for the RHCP and LHCP components of the electric field: (a) hexagon SHA for  $\varphi = 0^\circ$  at the right-hand state, (b) hexagon SHA for  $\varphi = 90^\circ$  at the right-hand state, (c) hexagon SHA for  $\varphi = 0^\circ$  at the left-hand state, (d) hexagon SHA for  $\varphi = 90^\circ$  at the left-hand state, (e) square SHA for  $\varphi = 0^\circ$  at the right-hand state, (f) square SHA for  $\varphi = 90^\circ$  at the right-hand state, (g) square SHA for  $\varphi = 0^\circ$  at the left-hand state, and (h) square SHA for  $\varphi = 90^\circ$  at the left-hand state.

The gain of helical antennas operating at the axial mode depends on the number of turns. Specifically, the gain increases as the number of turns increases. However, the gain

**TABLE 4.** Simulated gain versus number of turns of the bifilar skeleton SHA.

Number of Turns	2	4	6	8	10
Hexagon SHA Gain (dBi)	9.94	11.5	13.23	14	14.38
Square SHA Gain (dBi)	9.85	11.27	12.85	13.64	14.04

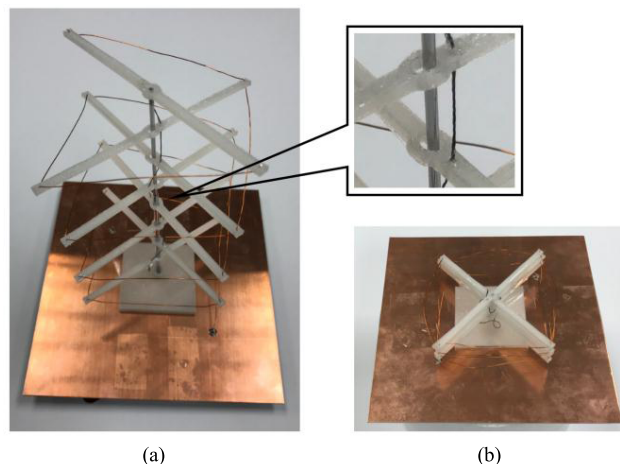


**FIGURE 15.** (a) Deployable skeleton scaffolding for square SHA. (b) Compressed square skeleton SHA.

does not increase linearly with the number of turns. In fact, for a large number of turns, an increase in the number of turns does not necessarily result in more directional radiation pattern [23]. Practical helical antennas have 5 to 15 turns. Table 4 shows the variation of the simulated gain versus the number of turns of our bifilar skeleton SHAs. From these simulation results, it is observed that increasing the number of turns beyond 10 turns does not significantly increase the gain of the SHAs. Also, higher gain can be achieved by using a reflector [14] or helical antenna arrays [24].

The skeleton based SHA is also a collapsible and deployable antenna like the origami SHA. A supporting mechanism is developed, as shown in Fig. 15. Specifically, the hollow cylinders between the arms were removed and an additional hole was drilled on each PLA arm. The position of this hole is close to the central axis. A nonconductive thread is fed through the holes, and the thread is fixed on each arm. The thread pulls the arms upward sliding them along the central post when the antenna is expanded, and also sets the distance between adjacent arms. A telescoping metal post is used as the central axis. This design structure allows the antenna arms to rotate and the antenna to collapse or expand its height. The telescopic tubular mast system [25] can be used to deploy the antenna automatically in space. The minimum collapsed height of this skeleton SHA, shown in Fig. 15(b), is approximately 17 mm, which make the antenna occupy 90% smaller volume compared to the volume of the completely expanded SHA. This is very useful for satellite antenna systems, where



the SHA can be collapsed and stowed compactly during launch while it can expand when it reaches space.

## VI. CONCLUSION

In this article, new designs of bifilar segmented helical antennas with switchable sense of polarization are presented based on origami and skeleton scaffoldings. The design parameters of the two structures are discussed. Both SHAs exhibit high directional gain and circular polarization as conventional helical antennas. However, the proposed SHA designs have the following unique advantages: 1) their sense of circular polarization can be switched from LHCP to RHCP by mechanical rotation around their central axis, and 2) they can collapse to achieve high efficiency packing ratios. These features make the proposed designs particularly useful for small satellites, e.g., CubeSats.

## REFERENCES

- [1] H. L. Knudsen, "Radiation field of a square, helical beam antenna," *J. Appl. Phys.*, vol. 23, no. 4, pp. 483–491, Apr. 1952.
- [2] J. P. Casey and R. Bansal, "Square helical antenna with a dielectric core," *IEEE Trans. Electromagn. Compat.*, vol. EMC-30, no. 4, pp. 429–436, Nov. 1988.
- [3] M. C. Britton, J. S. Wight, and P. C. Strickland, "Low-cost square cross section helical antennas," in *Proc. Symp. Antenna Technol. Appl. Electromagn.*, Winnipeg, Canada, Jul. 2000, pp. 425–428.
- [4] Y. S. Wang and S. J. Chung, "A miniature quadrifilar helix antenna for global positioning satellite reception," *IEEE Trans. Antennas Propag.*, vol. 57, no. 12, pp. 3746–3751, Dec. 2009.
- [5] M. B. Young, K. A. Connor, and R. D. Curry, "Reducing the size of helical antennas by means of dielectric loading," in *Proc. IEEE Pulsed Power Conf.*, Chicago, IL, USA, Jun. 2011, pp. 1–5.
- [6] R. M. Barts and W. L. Stutzman, "A reduced size helical antenna," in *Proc. IEEE Antennas Propag. Soc. Int. Symp.*, Jul. 1997, pp. 1588–1591.
- [7] S. A. Nauroze and M. M. Tentzeris, "A novel printed stub-loaded square helical antenna," in *Proc. IEEE Antennas Propag. Soc. Int. Symp.*, Vancouver, BC, Canada, Jul. 2015, pp. 774–775.
- [8] A. Takacs, N. J. G. Fonseca, H. Aubert, and X. Dollat, "Miniaturization of quadrifilar helix antenna for VHF band applications," in *Proc. Loughborough Antennas Propag. Conf.*, 2009, pp. 597–600.
- [9] D. K. C. Chew and S. R. Saunders, "Meander line technique for size reduction of quadrifilar helix antenna," *IEEE Antennas Wireless Propag. Lett.*, vol. 1, no. 1, pp. 109–111, 2002.
- [10] S. Hebib, N. J. G. Fonseca, and H. Aubert, "Compact printed quadrifilar helical antenna with ISO-flux-shaped pattern and high cross-polarization discrimination," *IEEE Antennas Wireless Propag. Lett.*, vol. 10, pp. 635–638, 2011.
- [11] J. Rabemanantsoa and A. Sharaiha, "Size reduced multi-band printed quadrifilar helical antenna," *IEEE Trans. Antennas Propag.*, vol. 59, no. 9, pp. 3138–3143, Sep. 2011.
- [12] J. Constantine *et al.*, "UHF deployable helical antennas for CubeSats," *IEEE Trans. Antennas Propag.*, vol. 64, no. 9, pp. 3752–3759, Sep. 2016.
- [13] X. Liu, S. Yao, B. S. Cook, M. M. Tentzeris, and S. V. Georgakopoulos, "A reconfigurable origami axial-mode helical antenna," *IEEE Trans. Antennas Propag.*, vol. 63, no. 12, pp. 5897–5903, Dec. 2015.
- [14] X. Liu, S. Yao, and S. V. Georgakopoulos, "Frequency reconfigurable origami quadrifilar helical antenna with reconfigurable reflector," in *Proc. IEEE Antennas Propag. Soc. Int. Symp.*, Vancouver, BC, Canada, Jul. 2015, pp. 2263–2264.
- [15] C.-W. Hsu, S.-K. Lin, and Y.-C. Lin, "Dual-frequency dual-sense circular polarization on asymmetric crossed-dipole antenna," in *Proc. IEEE Antennas Propag. Soc. Int. Symp.*, Chicago, IL, USA, Jul. 2012, pp. 1–2.
- [16] X. L. Bao and M. J. Ammann, "Monofilar spiral slot antenna for dual-frequency dual-sense circular polarization," *IEEE Trans. Antennas Propag.*, vol. 59, no. 8, pp. 3061–3065, Aug. 2011.
- [17] M. Boti, L. Dussopt, and J.-M. Laheurte, "Circularly polarised antenna with switchable polarisation sense," *Electron. Lett.*, vol. 36, no. 18, pp. 1518–1519, 2000.
- [18] Y. Ushijima, E. Nishiyama, and M. Aikawa, "Circular polarization switchable microstrip antenna with SPDT switching circuit," in *Proc. IEEE Antennas Propag. Soc. Int. Symp.*, Toronto, ON, Canada, Jul. 2010, pp. 1–4.
- [19] E. Demaine and M. Demaine, *History of Curved Origami Sculpture*. Accessed: May 15, 2015. [Online]. Available: <http://erikdemaine.org/curved/history/>
- [20] E. Demaine, M. Demaine, and A. Lubiw, "Polyhedral sculptures with hyperbolic paraboloids," in *Proc. 2nd Annu. Conf. BRIDGES, Math. Connections Art, Music, Sci.*, Aug. 1999, pp. 91–100.
- [21] S. Yao, X. Liu, R. Schamp, and S. V. Georgakopoulos, "Polarization switchable origami helical antenna," in *Proc. IEEE Antennas Propag. Soc. Int. Symp.*, Jun. 2016, pp. 1667–1668.
- [22] S. Yao, X. Liu, and S. V. Georgakopoulos, "Segmented helical antenna with reconfigurable polarization," in *Proc. IEEE Antennas Propag. Soc. Int. Symp.*, San Diego, CA, USA, Jul. 2017, pp. 2207–2208.
- [23] W. Eakasit, "Helical antennas with truncated spherical geometry," M.S. thesis, Dept. Elect. Comput. Eng., Virginia Tech Univ., Blacksburg, VA, USA, 2000.
- [24] X.-Q. Li, Q.-X. Liu, J.-Q. Zhang, and L. Zhao, "16-element single-layer rectangular radial line helical array antenna for high-power applications," *IEEE Antennas Wireless Propag. Lett.*, vol. 9, pp. 708–711, 2010.
- [25] M. Mobrem and C. Spier, "Design and performance of the telescopic tubular mast," in *Proc. 41st Aerosp. Mechanisms Symp.*, May 2012, pp. 127–140.



**SHUN YAO** received the B.S. degree in electrical engineering from Shandong University, Jinan, China, in 2006, the M.S. degree in software engineering from Beihang University, Beijing, China, in 2011, and the Ph.D. degree in electrical engineering from Florida International University, Miami, FL, USA, in 2017.

He is currently a Research Assistant with the Electromagnetic Laboratory, Florida International University. His research interests include wireless power transfer systems, novel antennas, antenna measurement, and origami reconfigurable electromagnetic systems. He has been served as the Technical Reviewer of the IEEE TRANSACTIONS ON ANTENNAS AND PROPAGATION, since 2014.



**STAVROS V. GEORGAKOPOULOS** (S'93–M'02–SM'11) received the Diploma degree in electrical engineering from the University of Patras, Patras, Greece, in 1996, and the M.S. and Ph.D. degrees in electrical engineering from Arizona State University, Tempe, in 1998 and 2001, respectively. From 2001 to 2007, he was a Principal Engineer with SV Microwave, Inc., Since 2007, he has been with the Department of Electrical and Computer Engineering, Florida International University, Miami, where he is currently an Associate Professor.

His current research interests relate to wireless powering of portable, wearable, and implantable devices, novel antennas, and wireless sensors. He received the 2015 FIU President's Council Worlds Ahead Faculty Award, which is the highest honor FIU extends to a Faculty Member for excelling in research, teaching, mentorship, and service. He has been served as an Associate Editor for the IEEE TRANSACTIONS ON ANTENNAS AND PROPAGATION, since 2013.